© 2017. Published by The Company of Biologists Ltd | Journal of Experimental Biology (2017) 220, 634-644 doi:10.1242/jeb.148213

RESEARCH ARTICLE

Naturalistic path integration of *Cataglyphis* desert ants on an air-cushioned lightweight spherical treadmill

Hansjürgen Dahmen[1,*,‡], Verena L. Wahl[2,‡], Sarah E. Pfeffer[2], Hanspeter A. Mallot[1] and Matthias Wittlinger[2,3,*]

ABSTRACT

Air-cushioned spheres are widely used as treadmills to study behavioural and neurophysiological questions in numerous species. We describe an improved spherical treadmill design that reliably registers the path and walking behaviour of an animal walking on top of the sphere. The simple and robust set-up consists of a very light hollowed styrofoam ball supported by an air stream in a hollow half sphere and can be used indoors and outdoors. Two optical mouse sensors provided with lenses of 4.6 mm focal length detect the motion of the sphere with a temporal resolution of more than 200 frames s^{-1} and a spatial resolution of less than 0.2 mm. The treadmill can be used in an open- or closed-loop configuration with respect to yaw of the animal. The tethering allows animals to freely adjust their body posture and in the closed-loop configuration to quickly rotate around their yaw axis with their own moment of inertia. In this account, we present the first evidence of naturalistic homing navigation on a spherical treadmill for two species of *Cataglyphis* desert ants. We were able to evaluate with good precision the walking speed and angular orientation at any time. During homing the ants showed a significant difference in walking speed between the approach and search phases; moreover, they slowed down significantly as soon as they reached zero vector state, the fictive nest position.

KEY WORDS: Fast response treadmill, Optical mouse motion sensors, Ant navigation, Homing, Orientation behaviour

INTRODUCTION

For several decades spherical treadmills have been important tools in the study of neurophysiological and behavioural questions in many animals. To control the behaviour of walking animals on spherical treadmills two types of treadmills have been invented; a sphere actively rotated by two (Kramer–Kugel; Kramer, 1976) or four (Götz and Gambke, 1968; Varjú, 1975) servo-motors and an air-cushioned passive low-mass sphere that is rotated by the animal itself. In the first case the position of the animal on top of the sphere is recorded by some device and any deviation from the zenith position is fed back to the servo motors that rotate the ball to bring the animal back to the zenith position. In these devices the animal is completely free to move. The difficulty, however, is to make the electronic servo-path from the animal position detector to the motor position correction response fast and precise enough to keep the animal on top of the sphere. It has been concluded that for fast-starting, -stopping and -turning animals (e.g. cockroaches), it is impossible to keep the animals on the zenith of the servo-rotated sphere. In the second type of treadmill the animal is kept fixed on top of the sphere and rotates the sphere itself. Here, the sphere the animal is walking on must be supported with as low friction as possible. To our knowledge the first air-cushioned Styrofoam sphere used as a treadmill in experiments with *Drosophila* was invented by Erich Buchner (Buchner, 1976), with the motion of this small sphere registered optically. In other earlier treadmills the rotation of the ball was registered by two light wheels touching the sphere along its equator at right angles with respect to each other (Dahmen, 1980; Doherty and Pires, 1987; Ye et al., 1995), like in the classic PC mouse with a rubber sphere touching two easily rotatable axes with spoke wheels interrupting light barriers. Later, optical computer mouse sensors were used to register the sphere's rotation (Mason et al., 2001; Hölscher et al., 2005; Hedwig and Poulet, 2004; Lott et al., 2007; Seelig et al., 2010).

Most recently, the so-called FicTrac method has been introduced (Moore et al., 2014). The motion of an air-cushioned sphere is registered by a camera monitoring the movement of a locally unique contrast pattern applied to the sphere. The advantage of this method is that the position of the patterned sphere can be extracted by image-comparing techniques in absolute coordinates where errors do not accumulate in time. However, the sampling rate is limited by the frame rate of the camera, and good imaging of the sphere pattern has to be guaranteed, including proper illumination.

In this account we describe an improved air-suspended spherical treadmill design (see Materials and Methods) with an extremely lightweight white spherical Styrofoam shell. The air cushion is generated by an air stream let in through a single hole in the bottom of a hollow half sphere, the air cup, made of aluminium to prevent electrostatic loading of the Styrofoam sphere. The air stream can be provided by an inexpensive membrane pump in conjunction with a simple air vessel.

The treadmill can be configured as a closed- or open-loop device with respect to yaw of the animal. In the open-loop configuration the body orientation of the animal is kept fixed in space and the sphere is allowed to rotate about all three axes. In the closed-loop configuration the animal is allowed to turn with practically no friction about the yaw axis with its own moment of inertia. Thus very fast turns are allowed and can be monitored. In the closed-loop configuration yaw of the sphere must be inhibited. In both configurations the design of the tether allows the animal to adjust its posture comfortably on top of the sphere. Motion of the sphere is reliably registered by two optical mouse sensors provided with a distance-adjustable external lens. The sampling rate of theoretical 6 kHz is artificially reduced to ∼200 Hz to guarantee a stable rate, the spatial resolution of the motion recording is 0.16 mm. The speed of the sphere's surface is limited to 5.6 m s^{-1}. Last but not least,

[1]Department of Biology, University of Tübingen, Auf der Morgenstelle 28, Tübingen 72076, Germany. [2]Institute of Neurobiology, Ulm University, Helmholtzstrasse 10/1, Ulm 89081, Germany. [3]Institute of Biology I, Albert-Ludwigs University of Freiburg, Hauptstrasse 1, Freiburg 70104, Germany.
‡These authors are joint first authors

*Authors for correspondence (Hansjuergen.dahmen@uni-tuebingen.de; matthias.wittlinger@biologie.uni-freiburg.de)

M.W., 0000-0002-9484-0179

Received 15 August 2016; Accepted 28 November 2016

Journal of Experimental Biology

Journal of Experimental Biology (2017) 220, 634-644 doi:10.1242/jeb.148213

owing to the simple and robust hardware, the treadmill is easy to use indoors in the laboratory as well as outdoors in the field.

The most important question is whether animals on the treadmill show naturalistic behaviour. We chose the *Cataglyphis* desert ant that is well known for its robust homing behaviour. *Cataglyphis* desert ants are the true navigators of hot and dry North African deserts. When searching for food they cover large distances in the vast and open landscape to find dead insects or small arthropods that have succumbed to the torridity of the desert. The ants employ path integration, a form of vector navigation, to bring back the food item to the nest as quickly as possible. Like sailors before the advent of GPS navigation, the ants have to integrate angles steered and distances travelled during the entire foraging run and continuously compute their current position relative to their starting position (Müller and Wehner, 1988; Wehner and Wehner, 1990; Collett and Collett, 2000; Ronacher, 2008). Once they have found a food item they are extremely motivated to bring it to the colony and immediately start their homing run. Homing *Cataglyphis* ants swiftly run back to the nest on the beeline, the so-called home vector, which was acquired during the outbound run. Is it possible for the ants to navigate, or rather, path integrate, on the air-suspended spherical treadmill? And if so, how does their behaviour on the treadmill apparatus compare with their behaviour in the natural habitat?

MATERIALS AND METHODS

General considerations on treadmills

Forces and torques

When considering spherical treadmills we have to consider the forces and torques the animal applies on its path, applying discrimination between straight forwards motion and turns.

For forward motion on a sphere with the moment of inertia θ around an axis through its centre we compare the force the animal has to exert to accelerate its mass (M_{animal}) on flat ground with the force the animal has to exert to accelerate the sphere with radius R when tethered on top of the sphere. It can easily be shown that both forces are the same if:

$$\theta/R^2 = M_{animal}. \quad (1)$$

We call θ/R^2 the effective mass (M_{eff}) of the sphere. Ideally M_{eff}=M_{animal}. Because for a homogeneous sphere:

$$\theta_{sphere} = 0.4 M_{sphere} R^2, \quad (2)$$

a thin walled spherical shell:

$$\theta_{shell} = 2/3 M_{shell} R^2, \quad (3)$$

the ideal mass of the sphere the animal runs on should be:

$$M_{sphere} = 2.5 M_{animal}, \quad (4)$$

$$M_{shell} = 1.5 M_{animal}. \quad (5)$$

For most small animals like insects available Styrofoam balls are too heavy and therefore must be hollowed. We manufactured hollowed Styrofoam spheres of 3, 5, 10, 15, 20 and 50 cm diameter with masses of 0.07, 0.3, 1.7, 3, 8 and 85 g, respectively (see Fig. S1).

It might be expected that for small animals, like *Cataglyphis* ants with a body mass of 10 to 60 mg, a 5 cm sphere (300 mg) would be too inert by a factor between 30 and 5. Nonetheless, it turned out that they run quite well on such a ball. Moreover, flies (*Musca domestica*) run on a 5 cm ball, and even *Drosophila* on a 3 cm ball. For larger animals like mice a 20 cm ball of 8 g is actually too light, as is a 50 cm ball of 80 g for rats. In those cases the wall thickness needs to be increased.

For turns, the moment of inertia of the animal can be estimated by a horizontal rod of length L and mass M rotating about the vertical axis through its centre:

$$\theta_{rod} = ML^2/12. \quad (6)$$

The ratio $\theta_{shell}/\theta_{rod}$ for a 5 cm shell of 300 mg and a rod representing a *Cataglyphis* ranges from ∼3000 for a small ant (10 mg mass, 0.7 cm body length) to ∼100 for a large ant (60 mg, 1.5 cm). For studies of the yaw response of animals it is therefore desirable to give the animals the freedom to yaw by themselves with their own moment of inertia about the vertical axis (see 'Tethering', below).

Treadmill configurations

There are two possible configurations of the treadmill, an open and a closed loop with respect to yaw of the animal (a schematic drawing of the two configurations is given in Fig. S3).

In the open-loop configuration the animal is fixed in its azimuth and rotates the sphere around the yaw axis when it turns, whereas the visual surrounding does not change its azimuth with respect to the animal. The sphere must be free to rotate about all three axes. The disadvantage of this treadmill configuration is that especially small animals have to overcome the much larger moment of inertia of the sphere around the yaw axis compared with their own moment of inertia, as discussed above.

In the closed-loop configuration the animal is allowed to freely rotate about its vertical axis and to adjust its azimuth on top of the sphere. The advantage of this set-up is that the animal can rotate around the yaw axis with its own moment of inertia, which allows for natural quick azimuthal changes. In this configuration the sphere must be prevented from rotations about the yaw axis.

Spherical shell production

Precise Styrofoam spheres were produced by boiling standard Styrofoam spheres in an aluminium precision spherical mould for 3 to 15 min, depending on the size of the sphere. The mould consisted of two half-spheres of a slightly smaller diameter (−1 mm) than the raw balls. At ∼100°C the Styrofoam melts and the rest of the gas dissolved in the plastic material makes it expand so that the mould is filled to its spherical edges. After cooling the mould in cold water the two halves are taken apart and the precise sphere taken out and cut into two halves using a tensioned thin steel wire of 0.1 mm diameter, heated by an AC current regulated in order to control the temperature of the wire.

To hollow the sphere, most of the material of its two halves was cut out by hand using a heated loop of thin steel wire. To get a spherical shell as light as possible and with a wall thickness as equal as possible, one half of the precision mould was placed and precisely centred on a turntable (see Fig. S1). The turntable could be rotated about a vertical axis by a stepper motor, the rotation speed of which could be quickly and easily controlled over a wide range. A small heated steel wire loop was fastened on a small base that could be rotated about a horizontal axis that crossed the axis of the turntable exactly at the centre of the sphere.

The wire loop could be adjusted such that it was rotated along a circle of a slightly smaller radius than that of the mould along a longitudinal line of the latter (i.e. it was moved at a small constant distance from the mould wall at all elevations of the mould half-sphere). By putting the roughly hollowed Styrofoam half sphere into the mould, rotating the turntable, heating the loop, and adjusting it at

Journal of Experimental Biology (2017) 220, 634-644 doi:10.1242/jeb.148213

stepwise increased elevations, the rest of the material was cut out in rings down to a thin and light half sphere. The speed of the turntable and the heat of the steel loop have to be adjusted carefully so that the wire loop cuts out the material but does not melt too much of it. After hollowing, the two half spheres were glued together by as little as possible of a two-component epoxy glue (UHU plus), in precisely the same orientation relative to each other as they were cut into halves. In this way spheres of the following diameters and masses were produced (see Fig. S2): 3 cm, 0.07 g; 5 cm, 0.3 g; 10 cm, 1.7 g; 20 cm, 8 g; 50 cm, 85 g.

The air cushion

Our spherical shells are supported by a hollow half sphere, the air cup, made of aluminium to prevent electrostatic loading of the Styrofoam sphere. The air is let in through a single hole in the bottom, which is sufficient because Bernoulli forces keep the sphere in a stable position in the middle of the cup independent of the strength of the air stream. With a strong air stream the sphere is even sucked into the cup, and it is possible to turn the cup upside down and the sphere is kept in place and does not fall out. It is not necessary to blow in the air through several holes in the cup to provide a uniform air support. It may be difficult to control a more or less equal air stream through all holes, and in most cases the air stream leaving small holes with high velocity would produce noise. In addition, the light shell surface may work as a noise amplifier. With a relatively large hole in the bottom, the supporting air stream can be made very slow and free of noise. For spheres up to 20 cm diameter a sufficient air stream can be provided by an inexpensive membrane pump connected to an air vessel (for example, a plastic bottle with two holes in its cap). For spheres of up to 10 cm diameter the air cup should have a diameter ~1 mm larger than the sphere, for larger spheres it should be ~2 mm larger. The depth of the air cup should be slightly less than the radius of the sphere so that the equator of the sphere remains visible, which is of advantage for monitoring the ball's motion.

In the open-loop setup the air cup is simply set up horizontally. In the closed-loop setup the sphere must be prevented from yaw. For this purpose the air cup is tilted by about 10 deg. The sphere floats on the air cushion against two light disks that touch the sphere along the equator (see Fig. 1B–D). The disks are mounted on horizontally aligned thin steel axes with tipped ends that are supported by tip bearings normally used in alarm clocks. The horizontal position of the disks and thus that of the sphere in the cup can be adjusted by micro-manipulators (see Fig. 1B and Fig. S2B,C). The sphere can now rotate about all axes that lie in the plane of the two touch points of the wheels and the centre of the sphere but any rotatory component orthogonal to this plane is disabled (Fig. S3A,B). The two small wheels that prevent the sphere from yaw add ~2% to the moment of inertia in the case of a 5 cm sphere, and less for larger spheres.

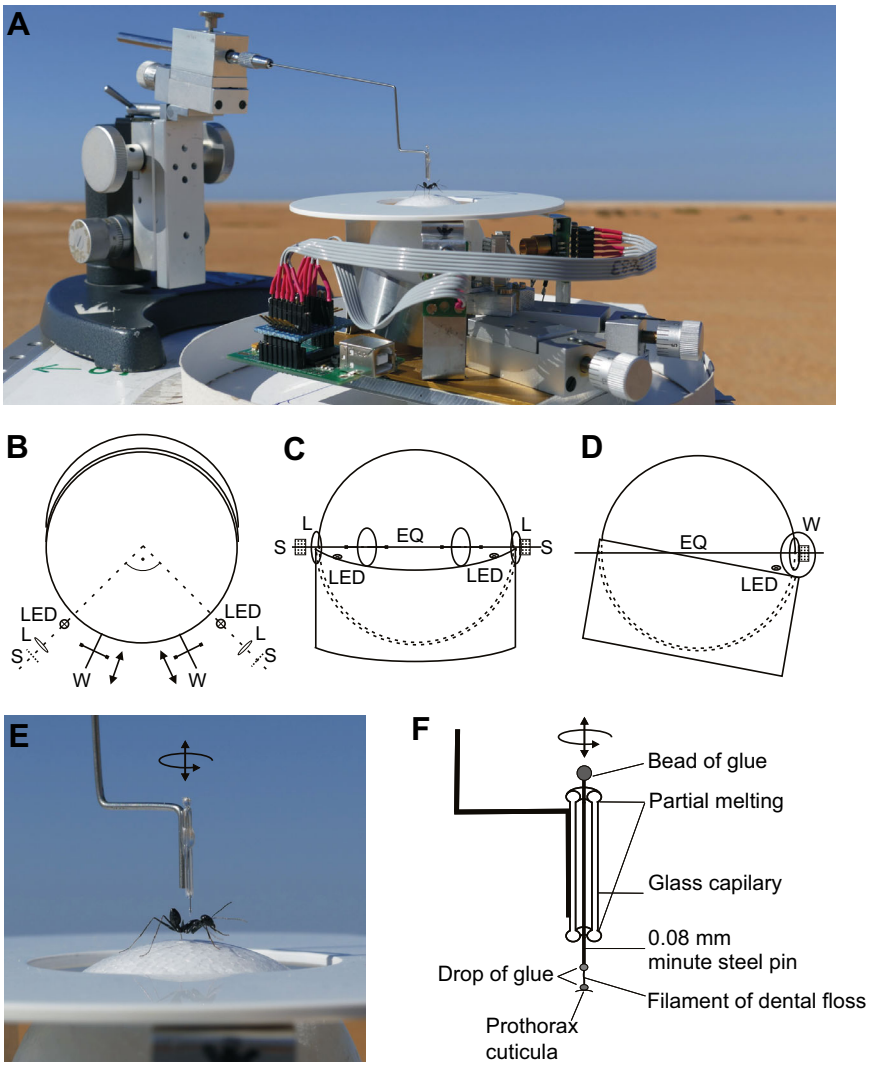

Fig. 1. Closed-loop system: experimental setup and animal tethering. (A) *Cataglyphis fortis* on the closed-loop treadmill with a styrofoam sphere of 5 cm diameter in the desert of Tunisia (complete overview). (B–F) Closed-loop configuration. (B) Top view, (C) front view, (D) side view. The air cup is tilted by 10 deg. Two wheels (W) are mounted on horizontal tip-supported axes and touch the sphere in the plane of its equator (EQ), thus preventing any yaw of the sphere. Motion of the sphere is monitored by two optical mouse sensors (S) that look at 90 deg of azimuth with respect to each other through lenses (L) to the equator of the sphere. Two somewhat tangentially shining LEDs enhance the contrast of the sphere surface sufficiently for safe sensor recordings. The two wheels can be moved horizontally (indicated by arrows in B) by micromanipulators, thus permitting centring of the sphere in the cup. (E) Prepared animal on the holder. (F) Schematic drawing of the holder of the closed-loop configuration.

Journal of Experimental Biology

Journal of Experimental Biology (2017) 220, 634-644 doi:10.1242/jeb.148213

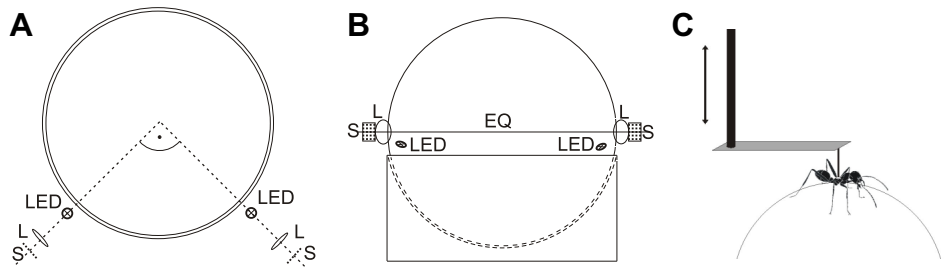

Fig. 2. Open-loop system: experimental setup and animal tethering. (A) Top view, (B) side view. The sphere is allowed to rotate about all three axes. The motion of the sphere is monitored by two optical mouse sensors (S) that look at 90 deg of azimuth with respect to each other through lenses (L) to the equator (EQ) of the sphere. Two somewhat tangentially shining LEDs enhance the contrast of the sphere surface sufficiently for safe sensor recordings. (C) Schematic drawing of tethering an animal by a small rod to a horizontal strip of paper. This way the animal is prevented from yaw and translation but allowed to adjust its height, roll and pitch to some degree on top of the sphere.

Tethering

In the open-loop configuration we successfully tethered small animals (mostly insects) using a horizontal strip of paper, one end glued to a short pin on the prothorax and the other to a vertical rod that could be adjusted in height by a micromanipulator (Fig. 2C). The paper strip allows the animal to move up and down on the zenith of the sphere, to roll and pitch slightly, but prevents any translation or yaw. For larger animals (mice and rats) we used a leather harness connected to a rotatable rod via a thin metal plate and two hinges as shown in Fig. 2D of Hölscher et al. (2005).

In the closed-loop setup the animal is glued to a 1–2 mm long single filament of dental floss (see Fig. 1E,F). The filament is attached to a fine steel rod of 0.08 mm diameter. The rod moves as a rotating axis in a ∼1.5 cm long vertical glass tube, the ends of which are melted slightly to provide a small hole with soft edges. This way the rod can be shifted up and down and rotated but horizontal motion is prohibited. The position of the glass tube is adjusted above the zenith of the sphere by a micromanipulator. The single filament acts as a ball joint. This way the animal is allowed to adapt its posture with respect to height, pitch and roll, and to rotate about the yaw axis with almost no friction. The animal can rotate around the yaw axis on top of the sphere with its own moment of inertia, which allows for extremely quick directional changes. However, when it moves forwards it is kept in place and rotates the sphere. The holes in the glass tube should be as small as possible and the length of the filament as short as possible so that horizontal clearance is kept small. We successfully glued *Cataglyphis* desert ants by hand without any anaesthesia to the 1 mm long single filament of dental floss with a fast UV-bonding glue (Bondic).

Registration of sphere motion

Any motion of the sphere in our treadmills was monitored by two optical mouse sensors (ADNS 3050, www.pixart.com), which look at 90 deg in azimuth with respect to each other through lenses to the equator of the sphere (Fig. 1B–D; Fig. S3). We selected our sensors from the large number of optical mouse sensor types available by the following criteria: a small form factor (eight DIP only), external LED illumination, separate data IN- and OUT-lines, and an operating voltage of 3.2 V, compatible with the operating voltage of many microprocessors. Our sensors contain a light-sensitive area of 0.75×0.75 mm in size with 19×19 quadratic pixels. In contrast to CMOS cameras the pixels in mouse sensors are comparatively large. The small number of pixels and the large light-gathering power allow for a much higher frame rate than with a CMOS camera. Automatic control of the shutter time adapts to variations of image brightness. In addition, a dedicated on-chip digital signal processor allows extraction of the dX- and dY-displacement between two reads and a Q-byte at a theoretical sampling rate of 6 kHz. The maximum allowed displacement speed (S_{max}) of the intensity pattern on the pixel array is 60 inch s^{-1}=1.524 m s^{-1}. The Q-byte allows evaluation of the 'quality' of the contrast in the image on the sensors' pixel array; the better the contrast the larger the Q-byte. A threshold on the quality Q-byte can be used to reject corresponding displacement result because of, for example, poor contrast of the image on the sensor surface. In the so-called 'pixel grab' mode, the image, i.e. the light intensity of each pixel on the sensor surface, can be extracted (see Fig. S6). This mode is very slow because for each pixel intensity a whole image must be sampled. To grab all pixel intensities of a whole image needs 19×19=361 samples. But this mode is essential to achieve the proper adjustment of the lens position.

Because of the short focal length of the factory-provided lenses, distance variations between the sphere surface and the mouse sensors might cause large fluctuations in recordings of the sphere rotation or even disable recording. Attaching a distance-adjustable lens of longer focal length in front of the sensor allows positioning of the sensor at a larger distance from the sphere surface and thus reduces to a large extent the sensitivity of the sensor response to these distance fluctuations. We used well-manufactured small aspheric plastic lenses of 4.6 mm focal length (F) with a relatively large numerical aperture of 0.4, designed by Phillips (CAY046) as collimator lenses for laser diodes. These small lenses have a good imaging quality, are light, inexpensive and easy to find.

The distance (G) of the lens to the sphere surface was ∼25 mm. This meant that fluctuations of the sensor response caused by fluctuations of the sphere distance of ∼1 mm are reduced to 1/25=4%. The image is demagnified by a factor V=(G−F)/F=4.44. Thus, the maximum detectable speed of the sphere surface is ∼6.76 m s^{-1} (=S_{max}×V). The spatial resolution is the smallest displacement of the sphere surface that leads to a change in the answer of the sensor by 1 count. In our case the minimal displacement of the sphere surface is (0.7/19)×V=0.16 mm, which corresponds to 6.12 counts mm^{-1}.

Attachment of a lens allows enlargement of the aperture in front of the sensor surface so that all the light through the lens can hit the sensor surface. The original aperture of 0.8 mm is situated somewhat oblique with respect to the sensor surface, reflecting the intended light path in the original illumination scheme of the PC mouse. We took off the cover of the sensor and drilled a slightly larger and properly side-shifted hole into it, so that the sensor area was open to all the light from the lens.

The sphere was illuminated somewhat tangentially from below or the side by an LED to enhance the contrast of surface irregularities of the sphere, as is normal for PC mouse chip setup. This permits the use of Styrofoam spheres without any pattern on the surface. We

normally use red LEDs for this purpose, but an infrared LED also works well, thus allowing the treadmill to be run in total darkness.

The responses of the PC mouse chips were read by a Cypress CY7C68013A-56P microprocessor with an onboard USB2.1 engine via seven general-purpose I/O pins (circuit diagram in Fig. S4). Because the five sensor-IN lines determine the timing and are common to the two sensors, reading the dX-, dY- and Q-bytes is done strictly synchronously and in parallel. The transfer of the six bytes via USB bulk transfer to a PC was performed by a small hex file on the microprocessor. The hex file was compiled from a 136-line C-program using a small device C-compiler (SDCC; https://sourceforge.net/projects/sdcc) and was loaded to the microprocessor via USB using FXLOAD (https://sourceforge.net/projects/libusb/libusb-1.0.21/examples). The sampling rate was artificially reduced to ∼200 Hz so that the Windows OS on the PC could accept the USB transfers and store the data at a stable rate. The program that controlled the type, storing and display of the USB data on the PC was also a simple 350-line C-code.

Details of the calibration of the sensors are described in Fig S4, the quality of the sensor response and the control procedure are reported in Figs S5, S6 and S7.

Behavioural experiments

Experimental situation and training

The experiments were performed with two different species of Cataglyphis desert ants, *Cataglyphis fortis* (Forel 1902) and *Cataglyphis bicolor* Fabricus 1793, and took place between June and July 2015 and in January and February 2016.

In the outdoor experiments (salt plains near Maharès, Tunisia, 34.53°N, 10.54°E) the ants were trained to walk a 10 m distance in their natural habitat from their nest entrance to a feeder located east of the nest. After successful training the ants were transferred to a flat and almost featureless remote test field to exclude all familiar olfactory, tactile or visual cues of the nest surrounding. The indoor experiments took place in the laboratory of Ulm University, Germany. Here, the foraging ants were trained to walk through an aluminium channel (7×7 cm) with a length of 4 m, which was illuminated by fluorescent tubes (daylight spectrum with UV, Solar Nature, JBL, Neuhofen, Germany) and covered with a linear polarizer filter (HN38 linear polarization film, 0.3 mm; ITOS GmbH, Mainz, Germany) that provided only the orthogonal polarization direction as compass cue. Because of space constraints in the laboratory the channel was set up with a 90 deg bend. As the orthogonal orientation of the polarizer filter with respect to the channel direction did not change over the entire length of the setup, the ants ignored the actual 90 deg bend and behaved exactly like animals trained in a straight channel (Lebhardt et al., 2012).

Experimental procedures and testing

Ants that reached the feeder and grasped a food crumb were then in the motivational state of homing and we thus refer to them as full-vector ants. For the homebound runs the full-vector ants in our experiments were grasped at the feeder and then the small filament of the tether was glued to their prothorax with the aid of the Bondic glue, which cures under UV light within a few seconds. A big advantage of this procedure is that the ants do not have to be anesthetized. The ants were then tested on the air-suspended spherical treadmill.

As soon as the tethered ants on the top of the treadmill grasp a food item and receive celestial or polarized light compass information (outdoor condition: open sky; indoor condition: polarizer filter and artificial light source) they start to perform a homing run, running off their full-vector to zero-vector state (Wehner et al., 1996). The outdoor experiments in Tunisia were performed with *C. fortis* (N=18, OUT-1). The experiments in the laboratory of Ulm were conducted with *C. fortis* (N=9, LAB-1) and *C. bicolor* (N=8, LAB-2). For comparison we tested homing runs of *C. fortis* recorded in an open test field (20 m by 20 m) in their natural habitat (N=20).

For all studies we used the closed-loop treadmill design shown in Fig. 1 (scheme in Fig. S3B) with a hollowed Styrofoam sphere of 5 cm diameter and a mass of 288 mg. The ants were able to freely rotate about their vertical axis very quickly on the top of the sphere (see also Movie 1). A white 5 cm high circular screen around the top of the treadmill prevented the ants from perceiving landmark and panoramic information but allowed for seeing large parts of the sky. This way we ensured that they could only rely on their path integrator to guide them home. The closed-loop treadmill was attached to a tripod stand, which enabled the apparatus to be turned in every direction. The 2D projection of the sensor's X and Y data were recorded in real time with 209 frames s^{-1}.

In the training site the feeder was located east of the nest. Hence, the apparatus was oriented westbound for testing the global home vector of foraging ants for the entire tracking time of 5 min in Tunisia, and 7 min in the laboratory.

Data analysis

Data were analysed in Matlab (MathWorks, Inc., Natick, MA, USA). To analyse the recorded trajectory we defined the first turning point as marking the position of the run, where the ant starts to differ from its current path direction for at least 30 deg and does not revert to its previous path direction for at least 3 m. We applied this criterion at a minimum distance of 5 m after the releasing point. With the aid of this turning point we separated the straight approach phase from the looping search phase of the ant's walk for the analysis (Merkle et al., 2006; Pfeffer et al., 2015).

With the information of the 209 data points per second, which contain the XY coordinates for every point, the corresponding in-time walking speed and angular orientation was calculated.

The angular orientation [alp(i)] was analysed for every data point (i) by means of the Matlab function atan2(Y,X) and π:

$$\mathrm{alp}(i) = (180\pi) \times \mathrm{atan2}((\mathrm{Y(i+k)} - \mathrm{Y(i)}), (X(i+k) - X(i)). \quad (7)$$

The walking speed [speed(i)] was calculated using the 209 data points per second:

$$\mathrm{speed}(i) = (\mathrm{sqrt}((Y(i+k) - Y(i))^2 + (X(i+k) - X(i))^2))/209. \quad (8)$$

Both were smoothed with k=100 (factor of 0.49). The angular speed was calculated as a rate of the change of angular displacement per second.

The search centre is the median position of all XY coordinates of the respective search loop or search phase. The index of straightness can estimate the tortuosity of trajectories and is calculated as the division of the straight line distance by the actual length of the trajectory. The accuracy of the nest search indicates how exactly the animals centre their search on the previous nest position. The width of search reflects how focused a particular search performance was and thus provides a measure of the ants' certainty regarding nest position (Pfeffer et al., 2015).

Journal of Experimental Biology (2017) 220, 634-644 doi:10.1242/jeb.148213

To analyse the response of straight-walking ants on the spherical treadmill to imposed changes of compass direction, and therefore a manipulated celestial compass, we tested ants trained to walk to a feeder east of the nest in the open field. We turned the entire apparatus back and forth under the open (and afterwards covered) sky. The starting orientation was westbound, corresponding to the ants' home vector. Before each turning of the apparatus [alternately right-hand (90 deg northbound) and left-hand (90 deg westbound)], we pushed a button to mark the start of turning the treadmill on the trace. We analysed the trajectories after this point to detect the turning points where the ant started to deviate at least 45 deg (the centre of the turn) from its current path direction (with respect to the apparatus) and did not revert to the previous path direction for at least 10 cm. To block celestial cues we used a paper board. The angular orientation with respect to the ant's current walking direction was calculated for N=16 turns with open and N=8 turns with covered sky for N=2 homing ants.

Statistical analysis

For statistical analysis and comparison the laboratory runs were normalized to 10 m vector length. We used SigmaPlot (Systat Software Inc., San Jose, CA) to generate box-and-whisker plots.

Owing to a sometimes relatively small sample size, we only used non-parametric tests. For independent data, we applied the Kruskal–Wallis ANOVA on ranks test (denoted as H-test) with the Dunn's method for *post hoc* multiple comparisons. For pairwise comparisons we used the Wilcoxon signed rank test for paired samples (denoted as Wilcoxon paired) and for multiple comparisons the Friedmann test with Bonferroni as *post hoc* correction. Data and program codes are available on request.

RESULTS

To show the practicability of this treadmill design we tested whether a complex but robust behaviour, such as path integration, can be performed and if it is comparable with the animals' natural behaviour in the open field. We tested homing *Cataglyphis* ants under open sky in Tunisia and in the laboratory setup of Ulm University.

The approach and search phases of homing runs are characteristic features that can be used to assess the quality of homing (Pfeffer et al., 2015).

Fig. 3A shows an example of a single homing run of *C. fortis* on the treadmill recorded under open sky in Tunisia. After running off the full-vector to zero-vector state [reaching the fictive nest site

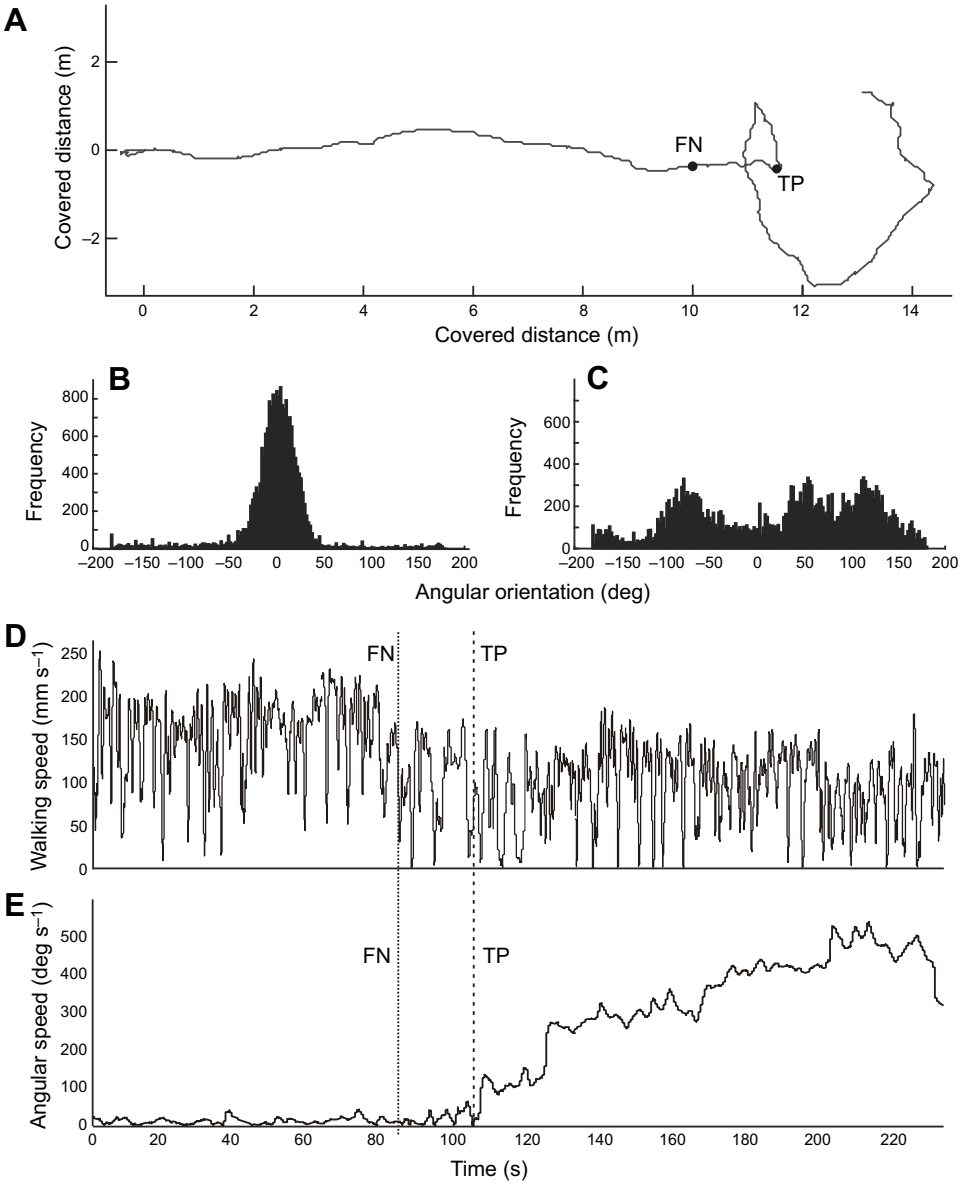

Fig. 3. Homing behaviour of a foraging ant: angular orientation and the walking speed separated into approach and search phases. Example of a tracked homing walk of the *C. fortis* ant after a training distance of 10 m. (A) Frequency histogram of the walking angle for (B) the approach phase before the turning point and (C) the search phase after the turning point (TP). (D) Walking speed plotted against the running time, approach phase (start to TP) with an average speed of 13.9 cm s^{-1} and the search phase (TP to end) with an average speed of 10.4 cm s^{-1}. The walking speed was smoothed with a moving average of a factor of 0.49. (E) Angular speed plotted against the running time, smoothed with a moving average of a factor of 2. The dotted line marks the time when reaching the 10 m point [fictive nest (FN)] whereas the dashed line indicates the turning point (TP).

Journal of Experimental Biology

Journal of Experimental Biology (2017) 220, 634-644 doi:10.1242/jeb.148213

(FN)] the ant's behaviour changes from a straight approach phase (Fig. 3B) to the looping search phase (Fig. 3C), which is indicated by a conspicuous turning point (TP) (Merkle et al., 2006).

Separating the mean walking speed of all runs with respect to the TP, the approach (0–TP) and search phase (TP–end) we can show a significant decrease of speed (Fig. 4A, left panel; Wilcoxon paired $P<0.001$). This reduction of walking speed can also be seen when the ants pass the position of the fictive nest site but when they still seem to be in the straight approach phase (see also Fig. 3D). This indicates that the walking speed was decreased at the FN (Fig. 3D, dotted and dashed line) and before the TP (Fig. 3D, dashed line). Separating the path at FN position shows a significant reduction of the mean walking speed (Fig. 4A, right panel, Wilcoxon-paired: $P<0.001$), irrespective of whether they showed a TP before or after the FN. This can also be observed when we separate the homing trajectories into three parts, depending on whether the ants first passed the fictive nest site while still running straight (Fig. 4B, left panel) or whether they turn (TP) before reaching the FN (Fig. 4B, right panel). During walking around curves the stride length of the inner side of the curve is shortened, whereas that of the outer side of the curve remains independent of the curvature (Zollikofer, 1994). Although there is a biomechanical coupling of linear speed and angular speed that depends on the radius of the curve, the decrease in speed in the data cannot be explained only by an increase in angular speed. When the ants, for example, take a sharp turn of 10 cm radius with a 10 mm distance between outside and inside footfalls at any given walking speed, they would only show a reduction of 5% walking speed resulting from the biomechanical coupling. The drop of walking speed that we show in the data is much larger (Figs 3 and 4, also compare Fig. S8); moreover, in Fig. 3D we can see that walking speed was already decreased at the FN (dotted line) and before the TP (dashed line), although the angular speed was not yet increased (Fig. 3E). In addition, in the search phase the speed is not only reduced during the times when turns occur but also during the times when the ants resume straighter walking in between the turns.

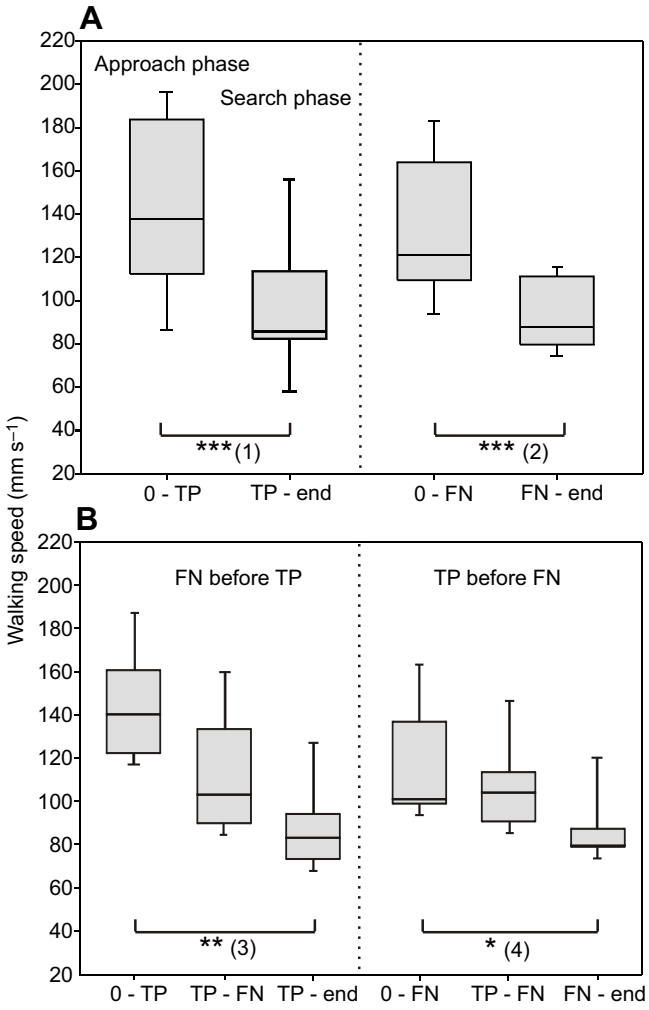

Fig. 4. Statistical analysis of the walking speed of tracked homing ants. (A) Walking speed of the homing runs of *C. fortis* under open sky separated into two phases according to the criterion of the first turning point (TP) (left panel, $N=15$) and separated by the fictive nest site position (FN) (right panel, $N=12$). (B) The homing runs are separated into three parts, depending on whether the ants first pass the fictive nest site before performing the TP (FN=10 m, left panel, $N=6$) or perform the TP before reaching the FN (right panel, $N=5$). Box-and-whisker plots give the 10th, 25th, 50th, 75th and 90th percentile distribution. Asterisks indicate statistical significance by the following analyses: (1) Wilcoxon paired, $P<0.001$; (2) Wilcoxon paired, $P<0.001$; (3) Friedmann test, $P=0.004$; (4) Friedmann test, $P=0.040$.

To compare the treadmill homing runs with open-field homing runs, we separated the approach phase from the search phase by means of the TP in the trajectories (Fig. 5) (Pfeffer et al., 2015). The length of the trajectories of the approach phase corresponds nicely to the nest-to-feeder distance (Fig. 5E) and is not significantly different between the experiments (*H*-test: H=3.016, $P=0.268$). We also found no significant difference between the experiments when we compared the distance of the first turning point with the pinpoint position of the fictive nest site (Fig. 5F; *H*-test: H=3.949, $P=0.389$). The ants tested in the laboratory setup showed a higher variability of the index of straightness (Fig. 5G; *H*-test: H=19.176; multiple comparison $P<0.05$ for Control versus LAB-2, OUT-1 versus LAB-1, OUT-1 versus LAB-2). For the search phase trajectories we determined the search centres that facilitate the comparison of the search behaviour of the tested groups (Pfeffer et al., 2015). It is noteworthy that the ants tested on the treadmill show a search behaviour that is less accurate compared with those tested in the open field. This means that the ants centre their search less on the position of the fictive nest site (Fig. 5H; *H*-test: $H=24.310$; multiple comparison $P<0.05$ for Control versus OUT-1, Control versus LAB-1, Control versus LAB-2). The width of search, which reflects how certain the animals are about the nest position, is not significantly different between the experiments. Nevertheless, the variability of the width of search is larger for the animals tested under artificial laboratory conditions (Fig. 5I; *H*-test: H=0.817, $P=0.845$). The 'loopiness' of the searches, as indicated by the index of straightness, tends to be largest in the open-field tested group, though it is not significantly different for all groups (Fig. 5J; *H*-test: $H=4.133$, $P=0.247$). The fact that all ants were holding on to their food item during the runs on the treadmill (and some ants even during the tethering procedure) proves that they were highly motivated to carry their food back home.

To see whether the ants respond to imposed changes of compass direction we manipulated the celestial compass input by actively turning the entire apparatus back and forth under the open (and afterwards covered) sky (Fig. 6). While turning the apparatus 90 deg back and forth the animals kept walking with a constant heading with respect to the celestial compass input as long as they saw the open sky. This results in a trajectory that shows 90 deg turns because the animals' walking direction changed with respect to the sensors (Fig. 6A,B). As soon as the sky was covered (black asterisk in Fig. 6A) we could not find such a compensation for directional change as the animals no longer had no access to the celestial compass information (Fig. 6A,C).

Journal of Experimental Biology

Journal of Experimental Biology (2017) 220, 634-644 doi:10.1242/jeb.148213

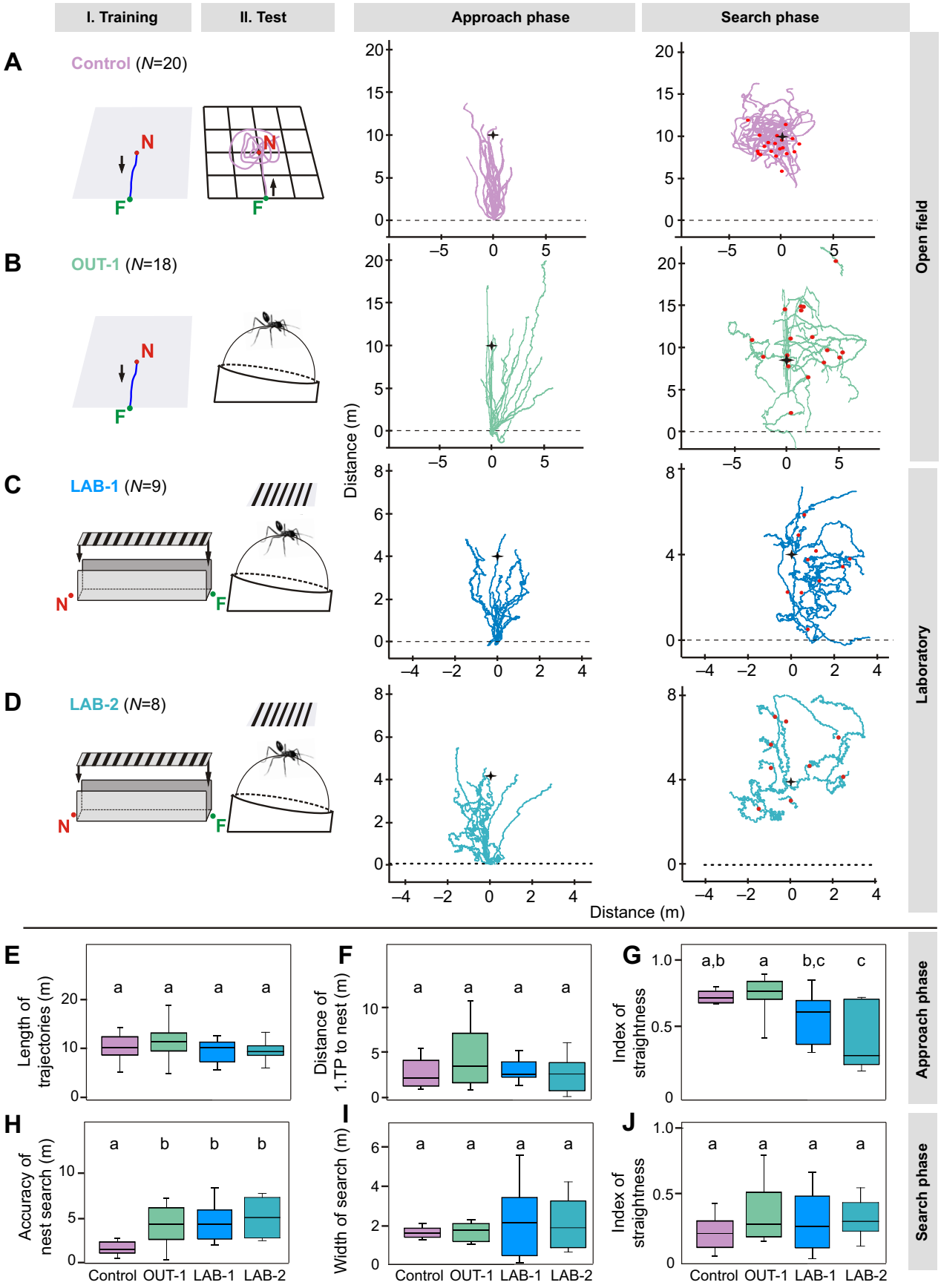

Fig. 5. See next page for legend.

Journal of Experimental Biology

Journal of Experimental Biology (2017) 220, 634-644 doi:10.1242/jeb.148213

Fig. 5. Approach and search phases of tracked homing walks of two different *Cataglyphis* species trained and tested under open-field or laboratory conditions. (A–D) First and second column show training and test setup for *Cataglyphis fortis* (A–C) and *Cataglyphis bicolor* (D). F, feeder position; N, nest position. Third column shows approach phases, fourth column shows search phases. For the third and fourth column, the trajectories of all ants have been superimposed; the first 20 m of the search phases are represented. The experiments in A and B were conducted under open sky in the desert of Tunisia. The animals were trained to visit a feeding site at a distance of 10 m. Homing runs were tested in an open test field (Control, *N*=20; A), and on the spherical treadmill (OUT-1, *N*=18; B). The experiments in C and D were conducted in the laboratory of Ulm. We trained the animal to walk to a feeding site through an aluminium channel of 4 m distance covered with a polarisation filter (represented as a black/white pattern) and tested their homing run on the spherical treadmill. (C) *Cataglyphis fortis* (LAB-1, *N*=9); (D) *C. bicolor* (LAB-2, *N*=8). A black cross marks the fictive nest position. The red dots show the search centres of every search phase. Corresponding analyses are shown for the approach phase: (E) length of the approach trajectories, (F) distance of first turning point to the nest, (G) index of straightness. For the search phase: (H) accuracy of nest search, (I) width of search, (J) index of straightness. For comparison, the laboratory data were normalised to 10 m distance. Box-and-whisker plots show the median as the box centre, plus 10th, 25th, 75th and 90th percentiles. Results of the statistical evaluation are indicated above the plots by letters; data sets with the same letters indicate an absence of significant difference, different letters indicate significant differences (for details, see text).

DISCUSSION

In our setup we wanted to demonstrate improvements to the well-introduced air cushioned sphere as a treadmill in studies on the orientation behaviour of animals that are fixed in space.

Improvements described are: (1) the production of lightweight spheres, (2) the use of air cups with a single and silent air inlet, (3) the reliable simple registration and calibration of the sphere's motion by optical mouse sensors with properly attached lenses, (4) high temporal (over 200 frames s^{-1}) and (5) spatial resolution (6 counts mm^{-1}), (6) the possibility to investigate open- and closed-loop orientation behaviour of animals mounted on top of the sphere, (7) the improved tethering of the closed-loop setup and (8) the easy transport and use of the device in outdoor environments.

The crucial improvement is the attachment of a distance-adjustable lens with a longer focal length than that provided by the manufacturer of the sensor chips. We show that mouse sensors prepared this way provide a fast and reliable registration technique that overcomes the criticisms of the mouse registration in, for example, Moore et al. (2014). However, the errors of mouse registration accumulate over time. Control of imaging and calibration are thus of great importance. When a single LED (or IR LED) illuminates the sphere, the normal irregularities of the Styrofoam surface provide enough contrast for the sensors to respond to any motion. No pattern on the sphere is needed.

Thanks to the mobile and robust design of the spherical treadmill (consisting of the treadmill device, a simple membrane pump driven from a battery, a plastic bottle as air vessel and a laptop computer), not only indoor but also outdoor experiments can easily be accomplished.

Owing to the high resolution of the spherical treadmill setup, we were able to study the homing runs not only spatially but also temporally with high precision.

The improved tethering of the closed-loop treadmill was essential for the comfortable posture of the animals, thus showing a naturalistic behaviour. For fast-turning animals like desert ants it is crucial that they can rotate around the yaw axis with their own moment of inertia (McMeeking et al., 2012).

The reconstructed paths on the spherical treadmill under open sky and in the laboratory are comparable with the homing trajectories

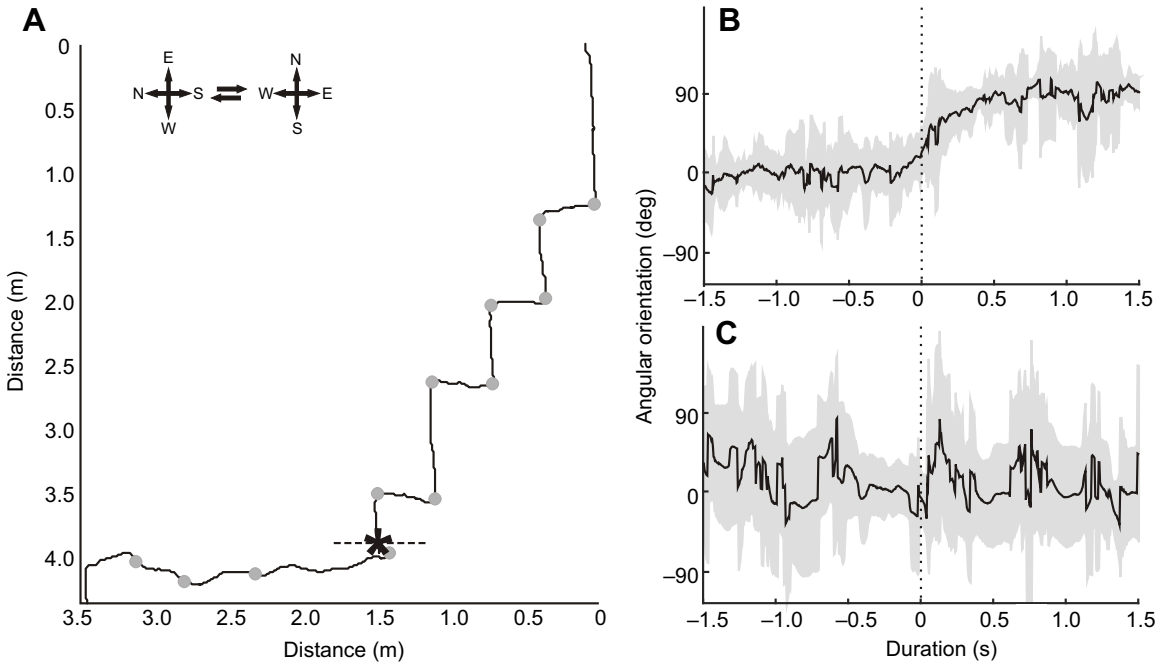

Fig. 6. Course correction response to imposed changes of the compass directions by turning the entire apparatus back and forth under the open sky. (A) Example of a homing run tracked on the spherical treadmill while alternately rotating the apparatus 90 deg to the right (northbound) and 90 deg to the left (westbound). The ant's starting position is at the zero point (0,0) and the ant initially moved westward towards its fictive nest position. The black asterisk marks the time when the sky was covered. The grey dots indicate the times when the apparatus was rotated. (B,C) The angular orientation with respect to the ant's current walking direction of *N*=2 homing runs with (B) open (*N*=16 turns) and (C) covered sky (no celestial information, *N*=8 turns). The dashed line indicates the centre of the turning behaviour of the ants. Turns to the left were mirrored and the angular orientations were smoothed with a moving average of a factor of 5. The bold black line indicates the mean value; the grey area marks the span of the standard deviation.

Journal of Experimental Biology

recorded in the open test field (Fig. 5A–D). The navigation and nest search performance is also comparable with results from *Cataglyphis* ants from previous decades (e.g. Wehner, 1982; Müller and Wehner, 1994; Åkesson and Wehner, 2002; Wehner et al., 2002; Merkle et al., 2006; Pfeffer et al., 2015) and also from Australian desert ant *Melophorus bagoti* (only nest search performance; Schultheiss and Cheng, 2011).

An interesting difference in our data is that the ants from captive laboratory colonies seem to show a less straight approach phase when running back to their nest site on the treadmill (Fig. 5G). A possible explanation might be the slower walking speed on the treadmill. In general the treadmill-tested groups performed less accurately in the nest search than the open-field-tested group (Fig. 5H). Although the precision or certainty about the nest position (width of search) is not significantly different between the groups the laboratory tested ants showed a larger variability within the width of search distribution (Fig. 5I). The ants from the laboratory do have plenty of food and no predatory pressure or heat stress (Wehner et al., 1992; Schmid-Hempel and Schmid-Hempel, 1984) so speed, accuracy and precision might not be so crucial. In the field we have highly motivated ants from wild colonies, higher temperatures and the celestial compass input is natural. Nevertheless, *Cataglyphis* ants from colonies kept in the laboratory are motivated enough to show typical path integration homing behaviour under artificial illumination.

Interestingly, homing ants that reached zero-vector state, the FN position, while they were still in the straight approach phase slowed down even before they started the looping search phase. Here, angular speed did not increase, suggesting that this drop in speed cannot be explained by a biomechanical coupling of linear and angular speed when walking around turns. In addition, ants that started the looping search phase before they reached the fictive nest slowed down at zero-vector state. The straight approach path and the looping search path show no difference in speed before reaching the FN. Previously, various measures for the first turn have been applied to determine when and where the ants 'think' they have reached their goal. The reduction of speed once the animals reach the fictive nest site can now be taken as a measure of the target probability function and therefore offers a new window to study path integration in more detail.

The possibility to investigate orientation behaviour of animals mounted on top of a sphere under natural closed-loop conditions allows us to analyse complex behaviour in great detail. We can say that *Cataglyphis* ants show typical homing behaviour, with a straight approach phase and looping search phase, and hence navigate in a naturalistic way under the artificial conditions on the treadmill.

In future applications, one could imagine many ways of manipulating the ants' surrounding visual or olfactory environment to investigate how it interacts with, for instance, path integration. The newly improved spherical treadmill is a valuable tool to better understand the remarkable features of the ants' navigational toolkit.

Acknowledgements
We gratefully thank Harald Wolf, Ulm University, for generous support. Hanspeter Mallot, Tübingen University, kindly supported the manufacturing of various versions of the treadmill by permitting H.D. to use the workshop, rooms and equipment. We thank Ursula Seifert for her help in organising the field excursions and for editing the text, Andrea Wirmer for statistical advice and Dennis Grüninger, Elena Haugg, Mario Hildebrand and Stephanie Offergeld for their help during the experiments.

Competing interests
The authors declare no competing or financial interests.

Author contributions
H.D. designed and developed the apparatus. H.A.M. provided crucial support for manufacturing the devices. M.W. and V.L.W. designed the experiments; M.W., V.L.W. and S.E.P. performed the behavioural experiments. V.L.W. and S.E.P. analysed the data. H.D., V.L.W. und M.W. wrote the manuscript, and H.A.M. revised the manuscript.

Funding
The University of Ulm and Eberhard Karls Universität Tübingen provided basic financial support and infrastructure.

Supplementary information
Supplementary information available online at
http://jeb.biologists.org/lookup/doi/10.1242/jeb.148213.supplemental

References
Åkesson, S. and Wehner, R. (2002). Visual navigation in desert ants Cataglyphis fortis: are snapshots coupled to a celestial system of reference? *J. Exp. Biol.* **205**, 1971-1978.
Buchner, E. (1976). Elementary movement detectors in an insect visual system. *Biol. Cybern.* **24**, 85-101.
Collett, M. and Collett, T. S. (2000). How do insects use path integration for their navigation? *Biol. Cybern.* **83**, 245-259.
Dahmen, H. J. (1980). A simple apparatus to investigate the orientation of walking insects. *Experientia* **36**, 685-687.
Doherty, J. A. and Pires, A. (1987). A new microcomputer-based method for measuring walking phonotaxis in field crickets (Gryllidae). *J. Exp. Biol.* **130**, 425-432.
Götz, K. G. and Gambke, C. (1968). Zum Bewegungssehen des Mehlkäfers tenebrio molitor. *Kybernetik* **4**, 225-228.
Hedwig, B. and Poulet, J. F. A. (2004). Complex auditory behaviour emerges from simple reactive steering. *Nature* **430**, 781-785.
Hölscher, C., Schnee, A., Dahmen, H., Setia, L. and Mallot, H. A. (2005). Rats are able to navigate in virtual environments. *J. Exp. Biol.* **208**, 561-569.
Kramer, E. (1976). The orientation of walking honeybees in odour fields with small concentration gradients. *Physiol. Entomol.* **1**, 27-37.
Lebhardt, F., Koch, J. and Ronacher, B. (2012). The polarization compass dominates over idiothetic cues in path integration of desert ants. *J. Exp. Biol.* **215**, 526-535.
Lott, G. K., Rosen, M. J. and Hoy, R. R. (2007). An inexpensive sub-millisecond system for walking measurements of small animals based on optical computer mouse technology. *J. Neurosci. Methods* **161**, 55-61.
Mason, A. C., Oshinsky, M. L. and Hoy, R. R. (2001). Hyperacute directional hearing in a microscale auditory system. *Nature* **410**, 686-690.
McMeeking, R. M., Arzt, E. and Wehner, R. (2012). Cataglyphis desert ants improve their mobility by raising the gaster. *J. Theor. Biol.* **297**, 17-25.
Merkle, T., Knaden, M. and Wehner, R. (2006). Uncertainty about nest position influences systematic search strategies in desert ants. *J. Exp. Biol.* **209**, 3545-3549.
Moore, R. J. D., Taylor, G. J., Paulk, A. C., Pearson, T., van Swinderen, B. and Srinivasan, M. V. (2014). FicTrac: a visual method for tracking spherical motion and generating fictive animal paths. *J. Neurosci. Methods* **225**, 106-119.
Müller, M. and Wehner, R. (1988). Path integration in desert ants, Cataglyphis fortis. *Proc. Natl. Acad. Sci. USA* **85**, 5287-5290.
Müller, M. and Wehner, R. (1994). The hidden spiral: systematic search and path integration in desert ants, Cataglyphis fortis. *J. Comp. Physiol. A* **175**, 525-530.
Pfeffer, S. E., Bolek, S., Wolf, H. and Wittlinger, M. (2015). Nest and food search behaviour in desert ants, *Cataglyphis*: a critical comparison. *Anim. Cogn.* **18**, 885-894.
Ronacher, B. (2008). Path integration as the basic navigation mechanism of the desert ant Cataglyphis fortis (Forel 1902) (Hymenoptera: Formicidae). *Myrmecol. News* **11**, 53-62.
Schmid-Hempel, P. and Schmid-Hempel, R. (1984). Life duration and turnover of foragers in the ant Cataglyphis bicolor (Hymenoptera, Formicidae). *Insectes sociaux* **31**, 345-360.
Schultheiss, P. and Cheng, K. (2011). Finding the nest: inbound searching behaviour in the Australian desert ant, Melophorus bagoti. *Anim. Behav.* **81**, 1031-1038.
Seelig, J. D., Chiappe, M. E., Lott, G. K., Dutta, A., Osborne, J. E., Reiser, M. B. and Jayaraman, V. (2010). Two-photon calcium imaging from head-fixed drosophila during optomotor walking behaviour. *Nat. Methods* **7**, 535-540.
Varjú, D. (1975). Stationary and dynamic responses during visual edge fixation by walking insects. *Nature* **255**, 330-332.
Wehner, R. (1982). Himmelsnavigation bei Insekten: Neurophysiologie und Verhalten. *Neujahrsblatt. Naturforsch. Ges. Zürich* **184**, 1-132.
Wehner, R. and Wehner, S. (1990). Insect navigation: use of maps or Ariadne's thread? *Ethol. Ecol. Evol.* **2**, 27-48.
Wehner, R., Marsh, A. C. and Wehner, S. (1992). Desert ants on a thermal tightrope. *Nature* **357**, 586-587.

Journal of Experimental Biology (2017) 220, 634-644 doi:10.1242/jeb.148213

Wehner, R., Michel, B. and Antonsen, P. (1996). Visual navigation in insects: coupling of egocentric and geocentric information. *J. Exp. Biol.* **199**, 129-140.

Wehner, R., Gallizzi, K., Frei, C. and Vesely, M. (2002). Calibration processes in desert ant navigation: vector courses and systematic search. *J. Comp. Physiol. A* **188**, 338-683.

Ye, S., Dowd, J. P. and Comer, C. M. (1995). A motion tracking system for simultaneous recording of rapid locomotion and neural activity from an insect. *J. Neurosci. Methods* **60**, 199-210.

Zollikofer, C. P. E. (1994). Stepping patterns in ants I. Influence of speed and curvature. *J. Exp. Biol.* **192**, 95-106.

Journal of Experimental Biology

SUPPLEMENTARY INFORMATION

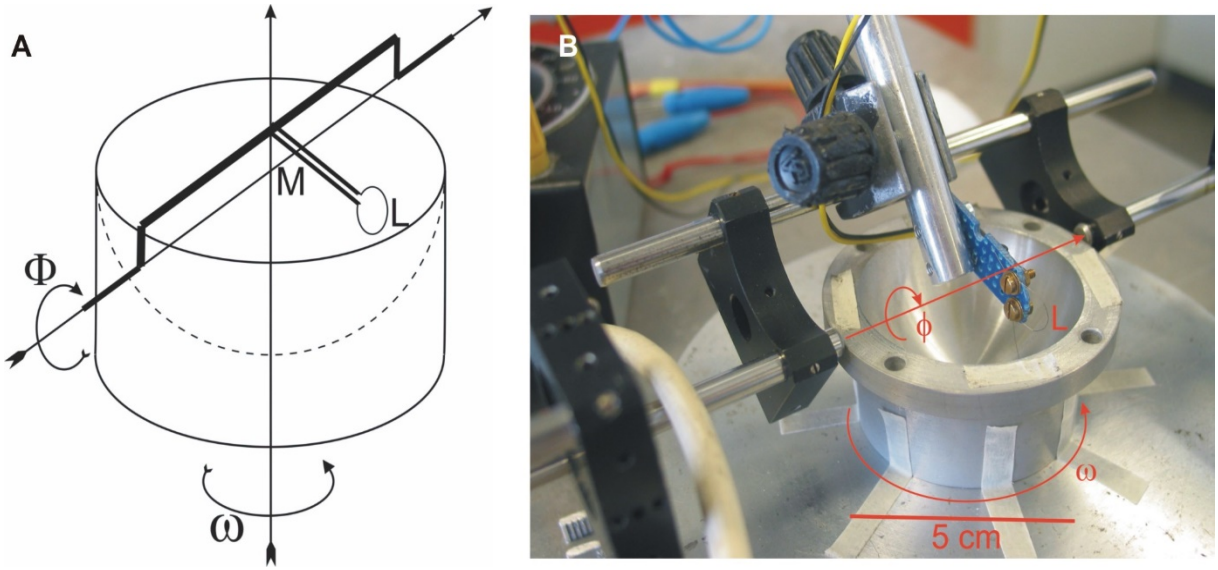

Fig. S1: Hollowing the Styrofoam sphere

To get a light spherical shell with equal wall thickness, a pre-hollowed half sphere was placed into one half of the precision mould precisely centred on a turntable. The turntable could be rotated about a vertical axis by a stepper motor, the rotation speed ω of which was carefully controlled. A small heated steel wire loop L could be rotated about a horizontal axis that crossed the axis of the turntable exactly at the centre M of the sphere.

The wire loop L was rotated along a circle of a slightly smaller radius than that of the mould along a longitudinal line of the latter (i.e. it was moved at a small constant distance to the mould wall at all elevations of the mould-half-sphere). Rotating the turntable, heating the loop, and adjusting it at stepwise increased elevations ϕ the rest of the material was cut out in rings down to a thin and light half sphere. The speed of the turntable and the heat of the steel loop have to be adjusted carefully so that the wire loop only cuts out the material but does not melt too much of it.

Journal of Experimental Biology • Supplementary information

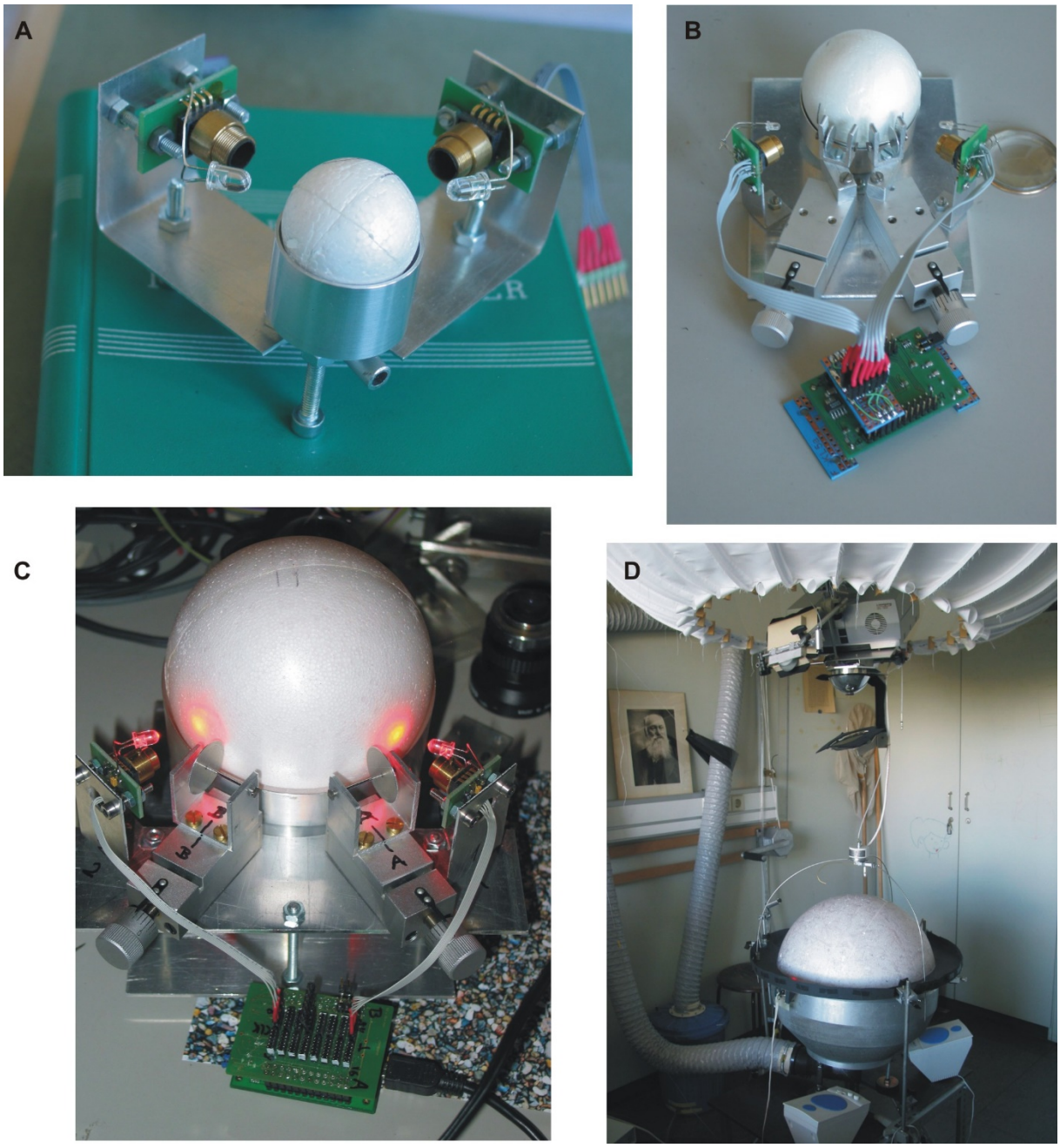

Fig. S2: Four Treadmill Examples

Four examples of treadmills are depicted: (**A**) a 3 cm and (**B**) a 5 cm sphere for smaller insects. (**C**) a 10 cm sphere intended for locusts and crickets (**D**) a 50 cm sphere for rats. In (**B**), (**C**), and (**D**) the sphere is prevented from yaw. (**A**) is an open loop configuration, (**B, C, D**) are closed loop configurations.

Journal of Experimental Biology • Supplementary information

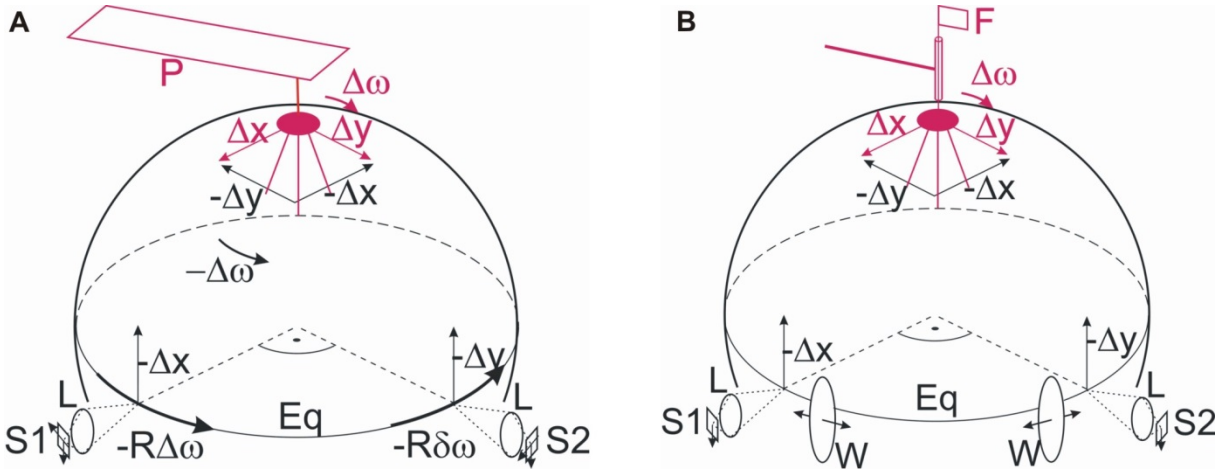

Fig S3: Schematics of the two possible configurations of the treadmill

Fig S3A shows the scheme of the open loop configuration, Fig S3B that of the closed loop configuration (the air cup was omitted). Both configurations are open loop with respect to translation: when the animal moves on the ground (i.e. the apex of the sphere) by a small distance Δx (Δy) it counter-rotates the sphere because of its tethering by -Δx (-Δy) which leads to a displacement of -Δx (-Δy) in the Y direction of sensors S1 (S2), respectively. But there is no visual feed-back to the animal's translation (besides of the small optic flow induced by the moving structure of the white sphere's surface underneath the animal).

The situation is different for yaw: In Fig. S3A the paper stripe P prevents any yaw of the animal and the sphere is free to rotate about all 3 DOFs. When the animal yaws on its ground by a small amount Δω it counter-rotates the sphere by –Δω but its orientation is kept fixed in space. This leads to a displacement of –RΔω in the X-direction of both sensors (R = radius of the sphere). But there is no visual feed-back to the animal induced by its yaw. This is an open loop situation with respect to yaw.

In Fig. 3B the animal is free to yaw with very little friction and its own moment of inertia. Any yaw of the sphere is prevented by the two wheels W. The consequence of the animal's yaw is immediately fed back to its visual system (and other organs), the yaw loop is closed. The apparatus does not respond to any rotation on the spot (besides of the rotation of the flag F). It only records changes in the running direction (and speed) of the animal with time- and space resolution described in the text.

Journal of Experimental Biology • Supplementary information

Reading the sensor response

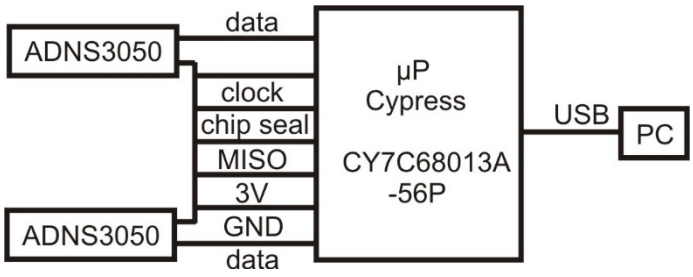

Fig. S4: Sensor-µP connections

Circuit diagram of the connection between the two mouse sensors ADNS3050 and the µP. The five In-lines of the sensors go to common GP Out pins of the µP, the two data out lines from the sensors to separate GP In pins. Thus the data transfer from both sensors to the µP is synchronous.

Sensor calibration

In order to calibrate the sensors' response in cm with the actual sphere, the latter is rotated by a weak extra air beam blown tangentially to the top of the sphere. The tip of a fine needle touches gently the sphere's surface in the centre of the visual field of say sensor one. In this way the sphere is forced to rotate about the axis through the tip of the needle and the centre of the sphere. Because the two sensors look at right angles to each other to the sphere's equator the sphere's motion in the visual field of sensor two is now vertical along a great circle through the zenith of the sphere. Recording the response to say 50 revolutions allows to calculate the response of sensor two to 1 cm of the sphere's motion. Sensor one is calibrated in the same way by touching the sphere by the needle in the visual field of sensor two. With our lens setup we get about 7-10 counts/mm depending on the actual distance of the sensors to the sphere's surface. Because the X- and Y -sensitivity are the same no X-calibration is necessary.

Journal of Experimental Biology • Supplementary information

Establishing the quality of the sensors‘ response

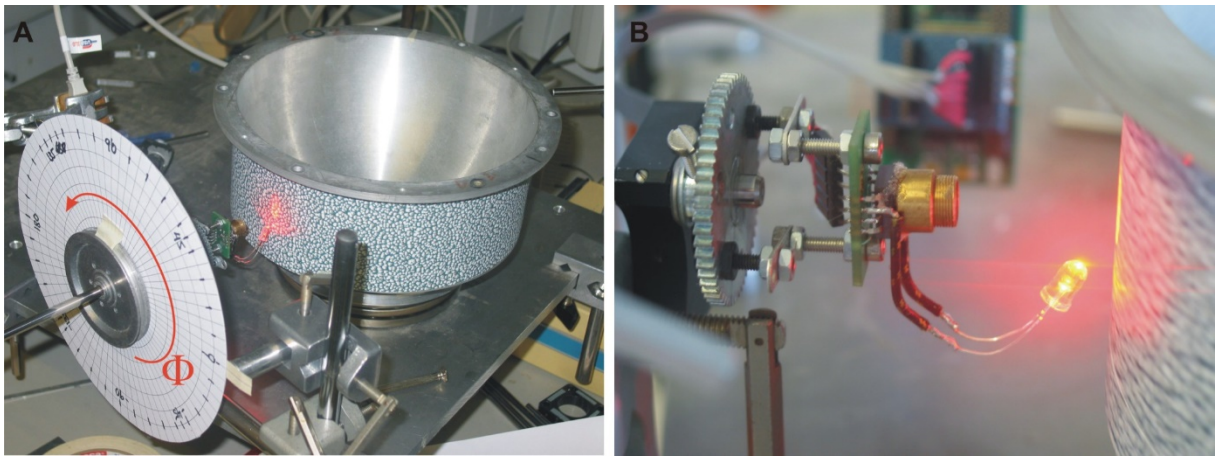

Fig. S5: Sensor response control: setup

(**A**) A vertical cylinder of 20.1 cm diameter was carefully centre on a table which could be rotated about a vertical axis by a stepper motor. A mouse sensor ADNS3050 with a 4.6 mm lens attached (see detail in (**B**)) looked along a horizontal axis to a contrasted pattern on the wall of the cylinder. The sensor could be rotated about its viewing axis by well controlled angles ϕ. The distance of the pattern to the frontal nodal point of the sensor's lens was 30 mm.

The quality of the sensor’s response

To judge about the quality of the sensors' motion recording we used a setup shown in Fig.S3. A motion sensor ADNS3050 with attached 4.6 mm lens and illumination LED looked along a horizontal viewing axis at right angles to the wall of a vertical cylinder of 20.1 cm diameter, carefully centred on a table which could be rotated by a stepper motor about a vertical axis (see Fig.S3A). To control the correct adjustment of the lens distance, the pattern of a 18pt large letter 'e' together with a set of stripes of 1mm distance (Fig. S4A) was attached to the wall of the cylinder and its image recorded in 'pixel grab' mode (Fig. S4B). From the stripes on the right edge of Fig. S4A we extract that the image of five stripes (distance = 4 mm) occupies about 16 pixels i.e. 16 x 0.75 / 19 = 0.63 mm. Thus the demagnification factor is about 4/0.63 = 6.33.

The distance of the wall to the frontal nodal point of the lens was about 30 mm (Fig: S3B). From the lens equation we conclude that the demagnification factor is therefore 30/4.6 = 6.5 which is in reasonable agreement with the estimate from the pixel image. We now attached a contrasted pattern to the cylinder wall shown in Fig. S3B and rotated the cylinder with a constant rotational speed of 13.4 sec per revolution which leads to a pattern speed of 4.72 cm/sec. We accumulated the dX-dY -responses of the sensor for various angular orientations ϕ of the sensor (Fig. S5A). We fit a straight line through the recordings of five cylinder-revolutions (316.25 cm) and plotted the slope against ϕ (Fig. S5C). The slope of the accumulated dX-responses should follow a cos (ϕ) function, that of the dY -responses a sin (ϕ) function. The plot shows the strict quadratic structure of the pixel array of the sensor, the sensitivities in X- and Y- direction are equal (see the equal amplitude of the slope at ϕ = 45° and -135°). The good fit of the Y -response to sin (ϕ) for ϕ around 0° and ±180° and that of the X-

Journal of Experimental Biology • Supplementary information

response to cos (ϕ) for ϕ around ±90° shows the excellent response of the sensor to slow optic flow. This is supported by Fig. S5B where the responses to the slowest flow in our series are depicted.

To test the sensor response for larger speeds we rotated the cylinder at pattern speeds from 4.72 cm/sec to 121.5 cm/sec. The theoretical speed limit for our demagnification factor of 6.33 is about 886 cm/sec. Because of the limited clock-rate of our stepper motor we could not reach that maximum. The time for 5 revolutions has been recorded by a stop watch by hand. Also the accumulated X-response for each cylinder-revolution has been stopped by hand. The result is presented in Fig. S5D. We conclude that within the hand stopping errors the accumulated X-response is the same for each revolution irrespective of the pattern speed.

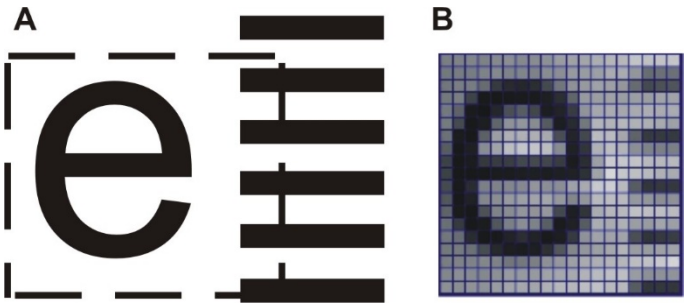

Fig. S6: Control of imaging quality

(**A**) Original and (**B**) 'pixel grab' of a 18pt large 'e'. The dark stripes at the right border are stripes and images of stripes with a line width of 0.25 mm and a distance of 1 mm. From the image of the stripes the demagnification factor of 1/6.33 can be extracted.

Journal of Experimental Biology • Supplementary information

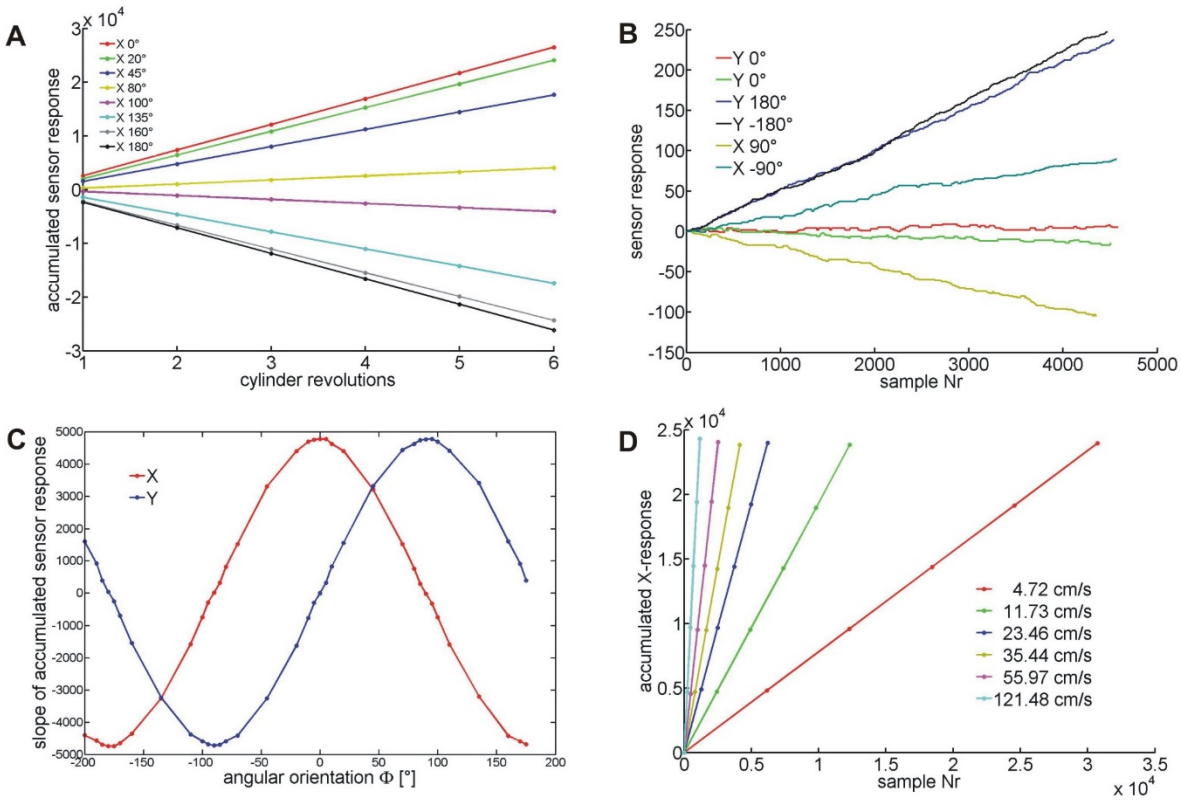

Fig. S7: sensor response control

(**A**) The sensors' accumulated X-response to selected angular orientations ϕ (see Fig. S3) versus the number of revolutions of the pattern cylinder. (**B**) The response to the slowest flow components in our sensor response control runs (please note the scale). (**C**) The slope of the sensor's accumulated dX-dY -responses plotted versus the angular orientation ϕ of the sensor. For ϕ = 0° the X-axis of the sensor is parallel to the pattern velocity. For further discussion see text. (**D**) The accumulated X-response to five cylinder-revolutions at various speeds. The response to each revolution is marked by a point. The X-response is independent of the speed of the pattern.

Journal of Experimental Biology • Supplementary information

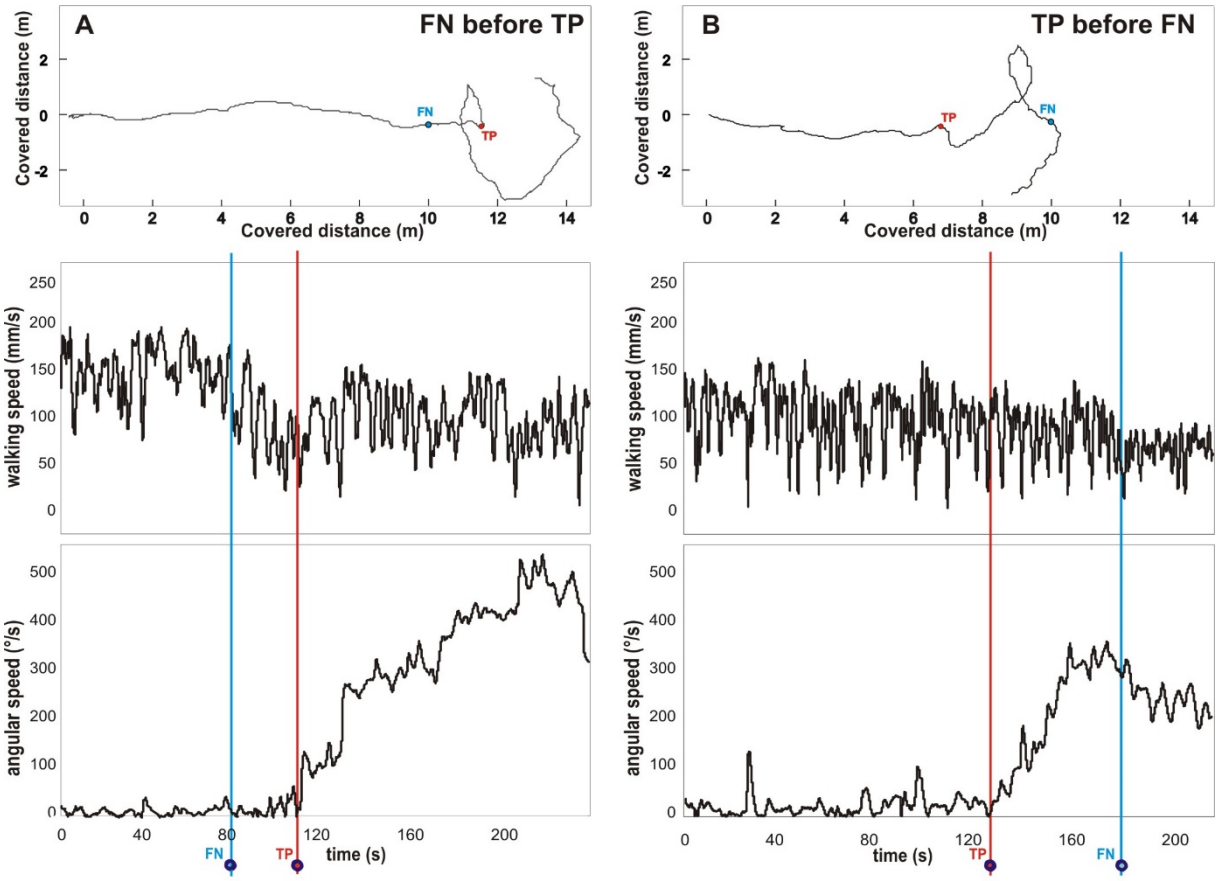

Fig. S8: Homing behaviour of two foraging *Cataglyphis fortis* ants with associated walking speed and angular speed

Example of two homing trajectories with (**A**) an ant first passing by the fictive nest position (FN, indicated as blue line) before showing a turning point (TP, indicated as red line) and (**B**) an ant showing the TP before passing by the FN. The walking speed was smoothed with a moving average of a factor of 1 and the angular speed was smoothed with a moving average of a factor of 2.

Journal of Experimental Biology • Supplementary information

SUPPLEMENTARY MOVIE

Movie S1

Example video of a homing *Cataglyphis fortis* desert ant on the closed loop setup.

Journal of Experimental Biology • Supplementary information